Bachelor's Project: Particle Physics

Comparing $\Lambda_b \to \Lambda\mu\mu$ and $\bar{\Lambda}_b \to \bar{\Lambda}\mu\mu$ decays at the $\psi(2S)$ resonance at the LHCb experiment

Author:
Mark Prirodins
S4763939

First Examiner:
Ann-Kathrin Perrevoort
Second Examiner:
Steven A. Jones

Faculty of Science and Engineering
University of Groningen
Groningen, the Netherlands
July 2025

Abstract

This work presents measurements of the raw asymmetry in the decays $\Lambda_b \to \Lambda\mu\mu$ via the $\psi(2S)$ resonance, using data collected by the LHCb experiment during Run 2 (2016–2018). The analysis is performed separately for different track types (LL, DD) and magnet polarities (MU, MD) as well as for the merged datasets, with special attention to background suppression and signal modelling. After applying selection criteria and fitting the invariant mass distributions, the raw asymmetry is extracted. The results show no sign of significant CP violation within the experimental uncertainties.

Contents

1 Introduction **3**

2 Theory **4**
2.1 The Standard Model . . . 4
2.2 CKM matrix . . . 5
2.3 LHCb . . . 6
2.4 Λ_b decay . . . 7

3 Method **9**
3.1 Combining the Data Sets . . . 9
3.2 Λ_b Candidate Selection . . . 9
3.3 Background Analysis . . . 10
3.4 Signal Modelling . . . 12

4 Results **16**

5 Discussion **18**

6 Conclusion **19**

7 Acknowledgements **20**

8 Appendix **21**
8.1 Error Propagation . . . 21
8.2 Figures and Tables . . . 21

References **22**

1 Introduction

The Standard Model (SM) is the most descriptive theory considering fundamental interactions and particles that humanity has developed so far. However, it fails to incorporate gravity, dark matter, and dark energy as well as to resolve the abundance of matter in our Universe. It is the latter question that is sounded in this work — why do we see baryonic matter only and not baryonic antimatter in nature? Baryon Asymmetry of the Universe (BAU) is a concept proposed by a Soviet nuclear physicist and human rights activist Andrei Sakharov in 1967 [1] as part of a set of conditions for baryogenesis currently known as the Sakharov conditions. In SM, matter-antimatter asymmetry is attributed to the violation of CP-symmetry. CP is a combination of Charge conjugation, the inversion of charges, and Parity, the inversion of spatial coordinates. It has been shown that the weak interaction is capable of breaking this combined symmetry [2]. The search for processes where the violation occurs might help advance our understanding of physics beyond SM.

The LHCb experiment at CERN is aimed at revealing the CP violation in processes involving b- and c-hadrons (i.e. particles that consist of quarks, some of which are b- or c-quarks) [3]. Hadrons of this composition are of special interest due to their high mass, which allows for rare decays to occur and to be distinguishable from the background. The exact decay considered in this work is $\Lambda_b \to \Lambda\mu\mu$ through $\psi(2S)$, an excited state of J/ψ or charmonium, composed of one charm- and one anti-charm quark [4]. To isolate this certain decay channel, the invariant mass of the produced muon pair is linked to the $\psi(2S)$ mass. The goal of this analysis is to calculate the raw asymmetry in the $\Lambda_b/\bar{\Lambda}_b$ decays at this specific energy. This raw asymmetry can arise from the production asymmetry at the primary vertex, where the protons collide, or during the decay via weak interaction. The result is also susceptible to the LHCb detector effects, which the author tries to mitigate by considering the data obtained for different configurations of the detector's magnetic field and for different categories of particle tracks recorded throughout the three years of Run 2 of LHC.

2 Theory

2.1 The Standard Model

The Standard Model (SM) is the most advanced theoretical model describing matter as such and the interactions of its smallest constituents in particular [5]. The table classifying the elementary particles in SM is given in the Figure 1. Fermions are the particles that are closest to the everyday understanding of matter, while their interactions are described using bosons, particles that carry interactions.

At present, it is believed that there are four fundamental interactions in nature: electromagnetic, the mediator of which is a boson called a photon, which has no rest mass and moves at the speed of light; strong interaction, which carries interactions between particles with the colour charge, the carrier of which, the gluon, also has the said charge and is massless like the photon; gravitational interaction, the theoretical carrier of which, the graviton, has not yet been included in SM; and weak interaction, which is of particular interest in this paper.

Fermions are characterized by the inability to exist in identical quantum states, which is called the Pauli exclusion principle. The quantum spin value, which describes the intrinsic angular momentum of a particle, takes half-integer values for fermions. Particles consisting of an odd number of fermions also have the properties of a fermion. Systems of an even number of fermions are close in their properties to bosons. They have an integer spin value and are described by the Bose-Einstein distribution.

Quarks and leptons belong to fermions. Their main differences lie in the charge they possess and the ability to exist outside of bound states. Quarks are incapable of existing separately and have a colour charge and a fractional electric charge. The colour charge ensures susceptibility to the strong interaction described by quantum chromodynamics (QCD). Colours are conventionally divided into red, green and blue, as well as their anti-colours. Such a designation uses the everyday understanding of colourlessness as a combination of RGB model components in equal proportions or as a colour-anticolor combination. QCD dictates the colourlessness of quark systems, which obliges them to exist in “colourless” combinations. The most common combinations of quarks in nature are baryons, consisting of three quarks, and mesons, consisting of quark-antiquark pairs.

Leptons can exist separately, since they do not have a colour charge. Their electric charge is an integer. Considering interactions other than the strong interaction, both quarks and leptons, except for neutrinos, are susceptible to all types. All fermions, including neutrinos, are subject to the weak interaction. Bosons of the weak interaction have significant mass, as well as the electric charge characteristic of leptons.

The property of the weak interaction investigated in this paper is CP symmetry violation (CPV). CP symmetry is the property of a system to remain unchanged under the action of C and P transformations. The C transformation (Charge conjugation) is the operation of inversion of the charges of the system. Effectively, this operation turns particles into the corresponding antiparticles. P (Parity) is the operation of reversal of spatial directions ($\vec{r} \to -\vec{r}$). Systems possessing CP symmetry remain unchanged, undergoing both operations simultaneously. The CPV is closely related to the models of the evolution of the Universe, in particular to the problem of the Baryon Asymmetry of the Universe (BAU).

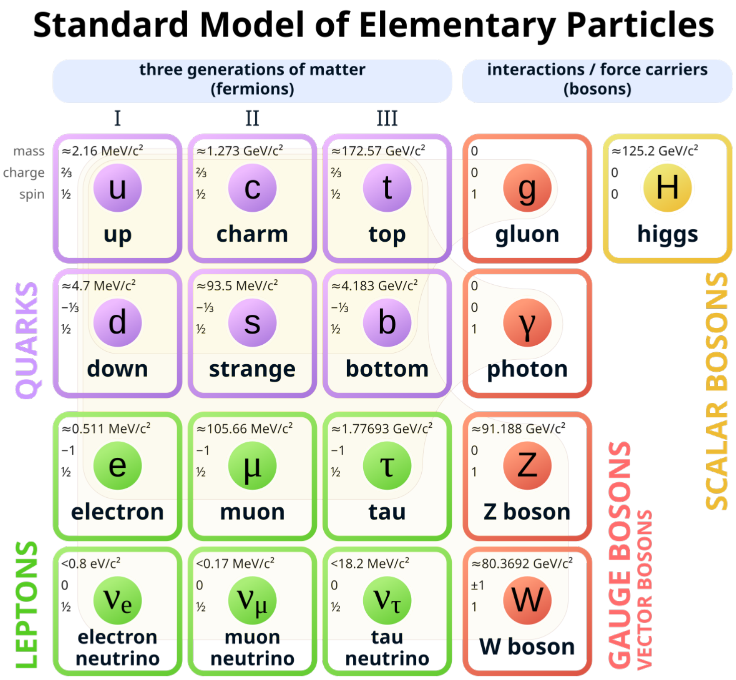

Figure 1: Standard Model of Elementary Particles [6].

2.2 CKM matrix

Quarks are divided into three generations. Each subsequent generation contains quarks heavier than the quarks of the previous generation. Each generation contains an up-type quark (up, charm, top) and a down-type quark (down, strange, bottom), which have the electric charge of $+\frac{2}{3}e$ and $-\frac{1}{3}e$, respectively. SM includes the possibility of quarks transforming into quarks of another type due to interaction with an electrically charged W boson. The most frequent transformations are observed between quarks of the same generation, but transitions between generations are also possible. These probabilities are described by the Cabibbo-Kobayashi-Maskawa (CKM) matrix (Equation 2.1 [7]). This 3×3 matrix has complex numbers as its elements, the squares of which describe the probability of transformation of one quark into another. The indices of the matrix element indicate specific transformation. The elements of the main diagonal are closest to one in absolute value, which reflects the predominance of intragenerational transformations. Antiquark transformations are determined by the elements of the conjugate CKM matrix.

$$\begin{pmatrix} d' \\ s' \\ b' \end{pmatrix} = \begin{pmatrix} V_{ud} & V_{us} & V_{ub} \\ V_{cd} & V_{cs} & V_{cb} \\ V_{td} & V_{ts} & V_{tb} \end{pmatrix} \begin{pmatrix} d \\ s \\ b \end{pmatrix} = V_{CKM} \begin{pmatrix} d \\ s \\ b \end{pmatrix} \tag{2.1}$$

If there is only one transformation channel for a quark and an equivalent channel for an antiquark, the probabilities of these transformations are equal, since the squares of complex conjugates are equal. If the transformation interferes with other channels, a difference in the complex phase of the CKM matrix can cause a difference in quark- and antiquark-transformation probabilities. The

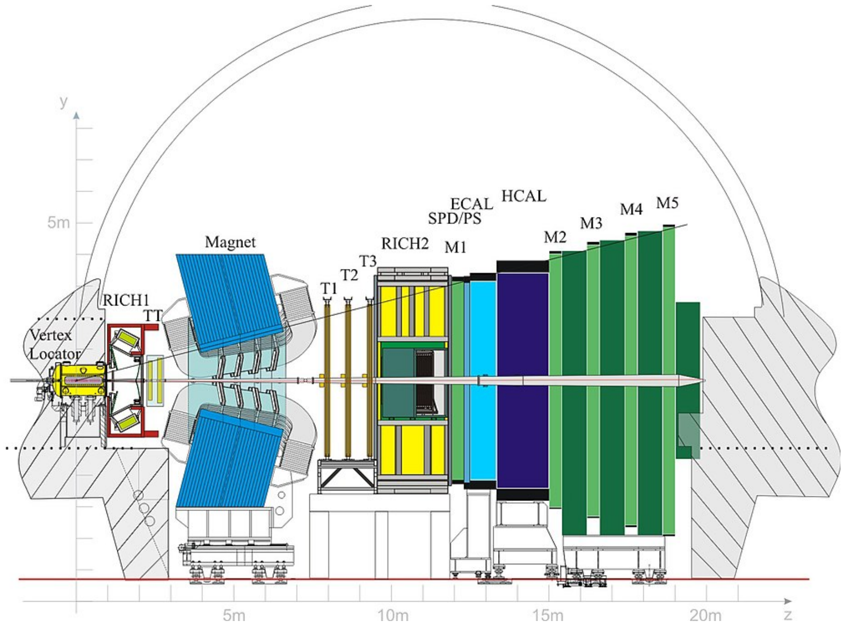

Figure 2: LHCb detector schematic [8].

mechanism of the complex phase of the CKM matrix describes CPV in the weak interaction. This mechanism, however, is considered insufficient for a full description of BAU, the predominance of matter over antimatter in the Universe. The magnitude of CPV in the weak interaction is significantly smaller than the value required to form a Universe dominated by matter to such an extent. It is thus necessary that SM is either modified to expand the possibilities for CPV or reformed completely to become what is now referred to as Beyond the Standard Model (BSM).

2.3 LHCb

The LHCb detector is one of the LHC experiments. This experiment aims at studying processes with b- and c-hadrons that occur in high-energy proton collisions. The b and c quarks are of interest because they are not part of the protons and also have a relatively large mass, which allows observing many, including very rare, decays. Such a richness of processes allows studying CPV.

The data used in this work were obtained during Run 2, namely the years 2016–2018, where the collision energy of 13 TeV and an integrated luminosity of about 2.5 fb^{-1} [9][10] were achieved.

The geometry of the LHCb detector (Figure 2) is aimed at recording the beam contained inside a conical region around the beam pipe with a vertex in the detector's Interaction Region. The detector systems lie in the pseudo-rapidity region of $2 < \eta < 5$, which corresponds to an angle between the beam beam axis and the cone generatrix of up to 250 mrad with a blind zone of 10 mrad around the beam axis. The detector is equipped with a dipole magnet, which allows spectrometry of particles by the curvature of their trajectories in a vertically directed magnetic field of 4 Tm. To avoid significant errors associated with asymmetric wear of the detectors, the polarity of the magnet is changed roughly biweekly, transferring it between the Magnet Up (MU) and Magnet Down (MD) states.

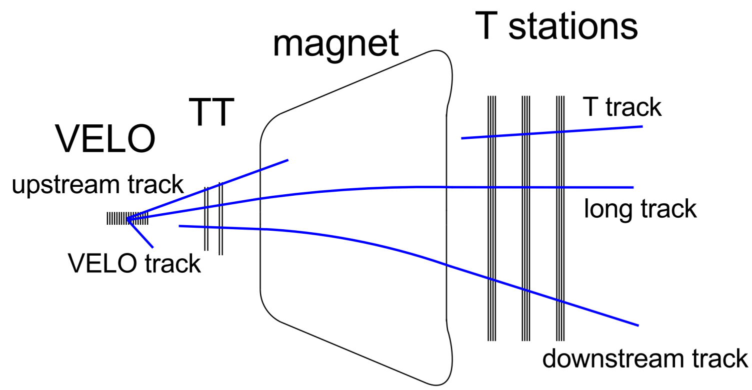

Figure 3: Tracks in LHCb detector [11].

The detector consists of many stacked subsystems. The Vertex Locator (VELO) system, closest to the Interaction Region, is dedicated to identifying the location of primary and registering secondary decay vertices of short-lived particles. This system is located at a distance of 8 mm from the Interaction Region. The next Trigger Tracker (TT) system allows registering particle trajectories before they enter the magnetic field. The particles encounter three more tracking systems at the exit from the magnetic field, after which the Cherenkov radiation detectors (RICH1, RICH2) record the radii of the light rings produced by the moving particles. This data is important for particle identification (PID). The final subsystems of the detector on the particle path are the electromagnetic calorimeters (ECAL) and hadron calorimeters (HCAL), which absorb electrons, photons and hadrons, as well as the muon detection system (M1 to M5).

When analyzing trajectories, five types of tracks are distinguished (Figure 3). The most informative are long tracks (LL), passing through all subsystems of the detector. They correspond to relatively long-lived states with significant momentum. The second category is Downstream tracks (DD), which are also long, but begin after VELO, therefore they are trajectories of secondary decay products. These tracks correspond to the long-lived particles that can be recorded throughout the detector volume. Upstream tracks belong to particles traced before the magnet zone in the VELO and primary tracking system TT. VELO tracks are interrupted after VELO and serve to reconstruct primary vertices. The last category, T-tracks, includes trajectories of particles detected only at tracking stations after the magnet. DD and LL tracks are analyzed in this work. The decay products p, π, μ are considered long-lived and can traverse the whole detector.

2.4 Λ_b decay

Λ_b is an electrically neutral baryon with spin $\frac{1}{2}$. The notation Λ_b reflects its association with the group of Λ baryons, which contain up and down quarks, as well as one of the heavier quarks, the bottom quark in this case (Table 1).

The particular decay analyzed in this paper produces the Λ^0 baryon and the $\psi(2S)$ meson, which is an excited state of J/ψ or charmonium ($c\bar{c}$) (Figure 4). The Λ^0 baryon decays into a proton-pion pair, where the pion carries a negative charge, and the $\psi(2S)$ meson decays into a muon-antimuon pair. A similar decay of $\bar{\Lambda}_b$ occurs with the production of $\bar{\Lambda}^0$, which decays into an antiproton and a positively charged pion, while the $\psi(2S)$ meson, being its own antiparticle in quark content, decays as in the case of Λ_b. The masses of Λ_b and its direct and secondary products are presented in Table 1.

Particle	Quark content	Mass, MeV/c^2
Λ_b	udb	5619.57 ± 0.16
Λ^0	uds	1115.683 ± 0.006
ψ(2S)	c$\bar{c}$	3686.097 ± 0.011
p	uud	938.27208816 ±0.00000029
π^-	d$\bar{u}$	139.57039 ± 0.00017
$\mu^\pm$	—	105.6583755 ± 0.0000023

Table 1: Λ_b and decay products [12].

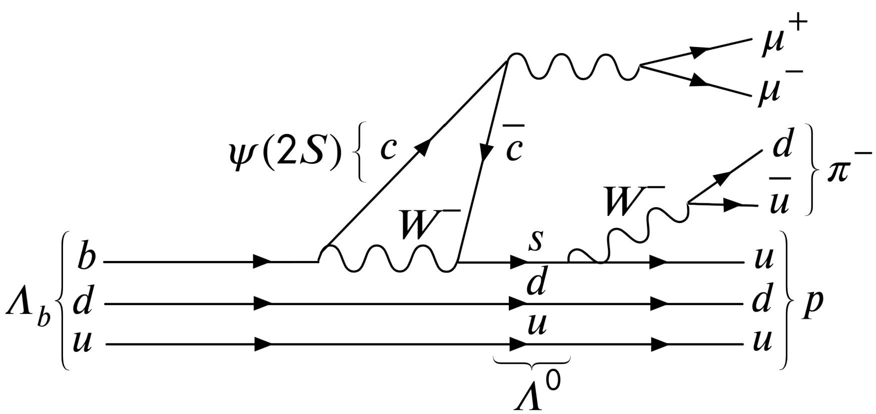

Figure 4: Λ_b decay scheme.

The asymmetry in the comparison of Λ_b and $\bar{\Lambda}_b$ decays is possible due to the production asymmetry in the primary vertex and presence of competing diagrams of the decay. The described process contains only one instance of the weak interaction, which, according to the mathematical considerations discussed earlier, should not contribute to the difference in the branching ratio. The presence of alternative channels, in turn, can cause interference, leading to asymmetry. The most significant contribution to the interference can be made by loop penguin diagrams [13].

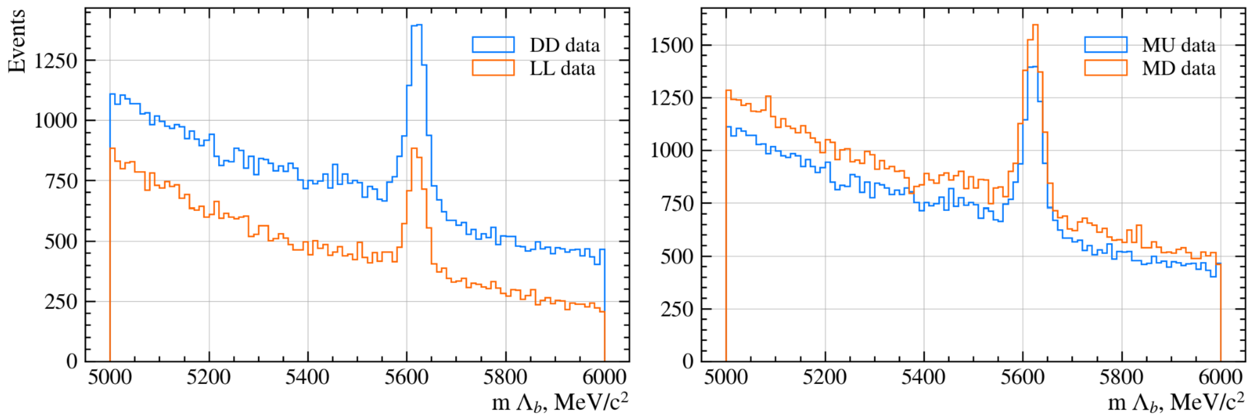

Figure 5: DD and LL dataset comparison (left), MU and MD dataset comparison (right).

3 Method

This paper presents an analysis of data from LHCb files spanning three years (2016–2018), two magnetic field polarisations (MU, MD), and two types of analyzed tracks (LL, DD). All data sets are combined for the final result. Data subdivision into DD and LL and further subdivision into DDMU, DDMD, LLMU, and LLMD sets is done for cross checking and error analysis. As the raw asymmetry is prone to the detector effects, the analysis of individual sets helps estimate their significance. It is, however, necessary to establish the feasibility of the data set merging first.

3.1 Combining the Data Sets

Different categories of sets are compared to check for differences in MU/MD or DD/LL data (Figure 5). The comparison is done on the Λ_b invariant mass distribution. The need for the data selection by the invariant mass is discussed further in this section, but the said selection is also necessary here to decide which data sets are compatible.

It is natural to expect no difference in MU and MD sets as they only differ in the magnet polarity, effectively curving charged particle trajectories in the opposite directions. The polarity is switched in order to mitigate errors that arise from the deterioration of the detector or other wear. In the final analysis, the efficiency of the detector cancels out when the count ratio is calculated. The difference in track types, however, proved to have more noticeable differences. LL track data shows a significantly lower number of events. Nevertheless, the overall shape is the same. To check for further differences, Monte Carlo (MC) simulations are compared, too (Figure 6). The two peaks show no significant offset, which allows to conclude no fundamental differences across the sets.

A more conclusive check is also made further in this section, where the MC simulation samples are modelled with a Gaussian distribution. Currently, the decision is made, as stated, to carry out the analysis both individually and in merged states.

3.2 Λ_b Candidate Selection

The data selected for the analysis corresponds to the signals inside the pseudo-rapidity region $2 < \eta < 5$ of the LHCb, explained previously. It is the part of the detector volume sensitive to the tracks analysed in this work.

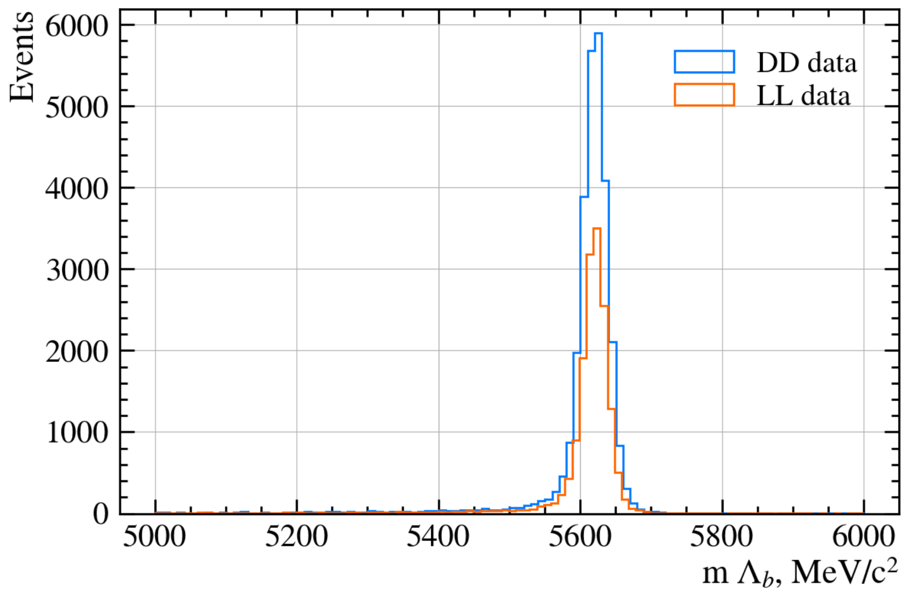

Figure 6: DD and LL Monte Carlo simulation comparison.

To isolate decays of Λ_b through the $\psi(2S)$ channel, several selection steps are taken. To ensure that production of $\psi(2S)$ occurs in the process, the muon pair produced in $\psi(2S)$ decay must be verified to carry the four-momentum q corresponding to the mass of the mother meson. More accurately, the square of the muon four-momentum transfer q^2 must be equivalent to the $\psi(2S)$ mass squared. Given the $\psi(2S)$ mass, it is reasonable to expect the decay to take place in the 13.6 MeV^2/c^4 region of q^2, which is further verified using both the Monte Carlo (MC) simulation and the experimental data (Figure 7).

The next step in separating the decay is to verify that the end products link back to Λ_b. This is done using the reconstruction of Λ_b invariant mass (Equation 3.1). MC simulation of the decay shows the Λ_b mass distribution peak around 5620 MeV/c^2, whereas a similar peak is seen the experimental data Λ_b mass histogram constructed from the Decay Tree Fitter (DTF) [14] data (Figure 8).

$$mc^2 = \sqrt{E^2 - (pc)^2} \tag{3.1}$$

3.3 Background Analysis

The application of both selection criteria on the full data set produces the Λ_b mass histogram seen in the Figure 9. It demonstrates a clear signal peak with a not too uniform background. The most of the background is showing a decay similar to the exponential function further referred to as the combinatorial background. Another type of background events manifests itself as a small bump at mass values of around 5500 MeV/c^2. To proceed with the modelling, it is important to identify this part of the background as it appears to overlap with the signal.

The bump in the background corresponds to the misidentified (misID) signals originating from the K_s meson decay. K_s is produced in the $B \to K_s\mu^+\mu^-$ event, decaying further through the

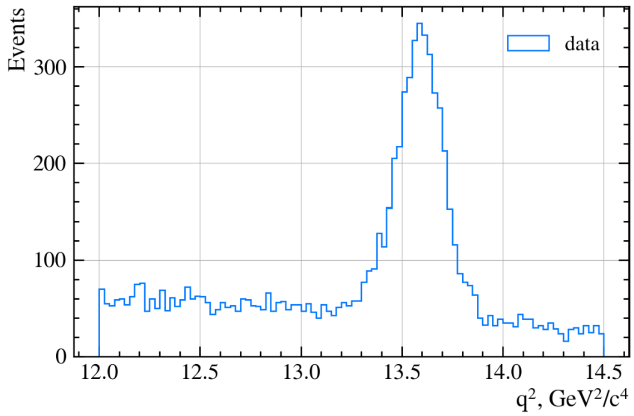

Figure 7: q^2 region corresponding to the $\psi(2S)$ decay in the experimental data (left) and MC simulation (right) sets.

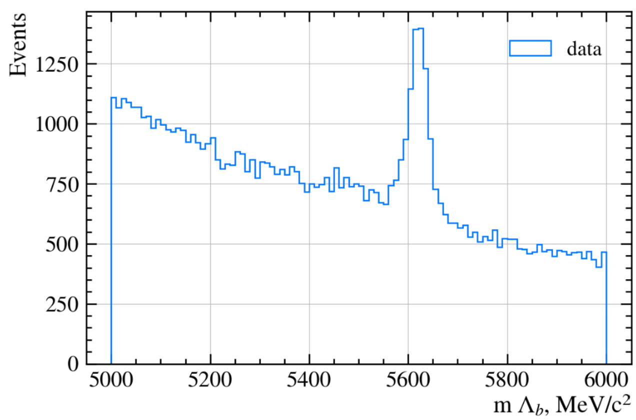

Figure 8: Λ_b invariant mass region for the experimental data (left) and MC simulation (right) sets.

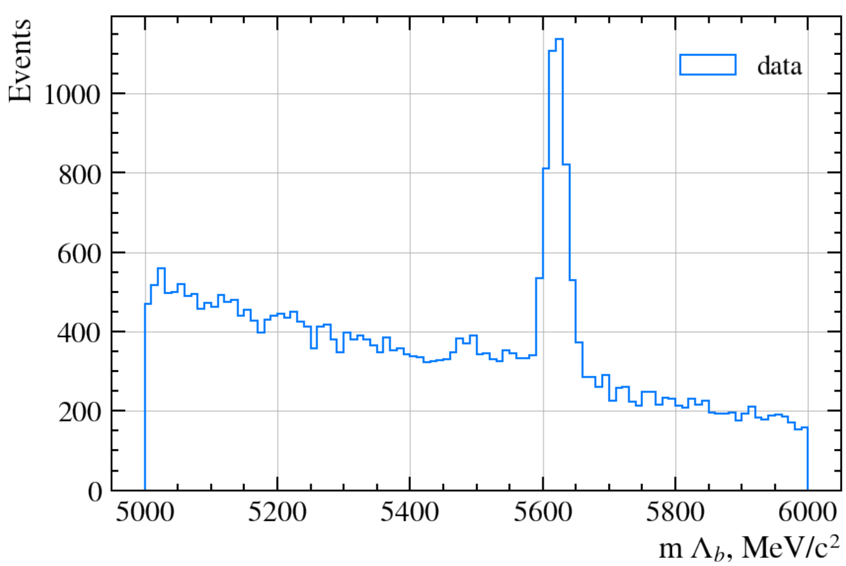

Figure 9: Full dataset with Λ_b mass and $\psi(2S)$ q^2 selections applied.

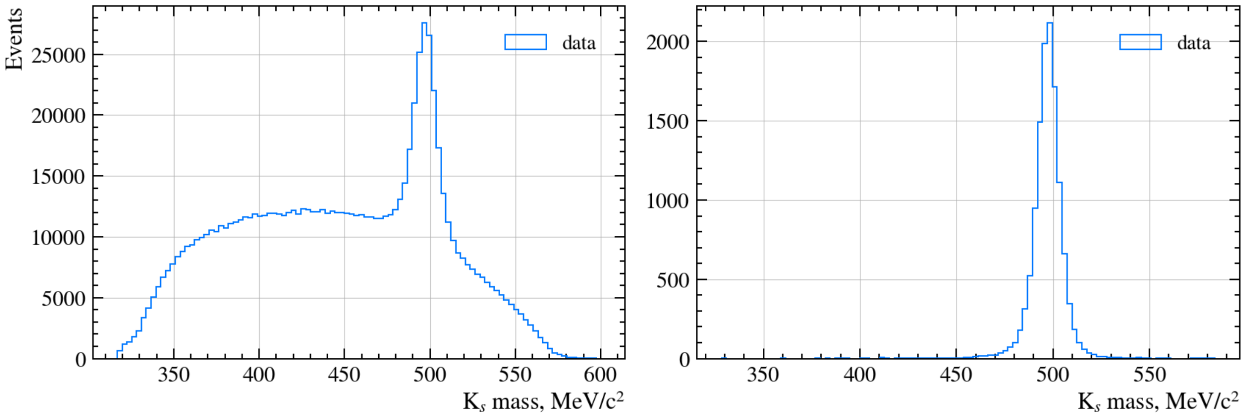

Figure 10: K_s invariant mass reconstruction with the mass of one of the pions substituted with the proton mass for the experimental data (left) and MC simulation (right) sets.

$K_s \to \pi^+\pi^-$ channel, where one of the pions is misidentified as a proton [15]. It is possible to imitate the misID signals using the K_s invariant mass reconstruction with the mass of one of the pions substituted with the mass of a proton. The reconstructed invariant mass histograms (Figure 10) for MC simulation and experimental data show a clear peak at around 500 MeV/c^2, which correlates with the K_s mass of 497.611 ± 0.013 MeV/c^2 [12].

To efficiently exclude the misID events from the final selection, the simulation is modelled as Gaussian distribution to extract the mean and the standard deviation of the peak. The decision to model the misID signals in this way is made due to the reduced χ^2 values of Gaussian fits being close to 1, more accurately, between 1.14 and 1.43 throughout all data sets. The Gaussian distribution parameters are used to exclude the events in the certain range around the centre of the misID signals distribution. The width of the cut is chosen to be 3 standard deviations around the mean. The effect of such a background suppression on the reconstructed invariant K_s mass data is shown in the Figure 11.

The histograms of Λ_b mass before and after the cut are shown in the Figure 12. The bump is not distinguishable from the combinatorial background; however, the number of events decreased noticeably even in the signal region. At the 3σ cut around the mean of the misID distribution, 77.45% of signal events are conserved, while also 4.50% of misID events remain. The high misID event count after suppression is attributed to the fact that the misID signal distribution diverges from the Gaussian further from the centre.

Having efficiently removed the bump overlapping with the signal, it is now possible to model the distribution. At this stage, the data undergoes the following selection (Table 2):

3.4 Signal Modelling

To fit the signal with a distribution function, Gaussian distribution is tested on the MC simulation samples. The reduced χ^2 test is employed to select the best fitting parameters for each dataset. The outcomes of this test are visualised in the Figure 13 utilising two-dimensional distributions. In

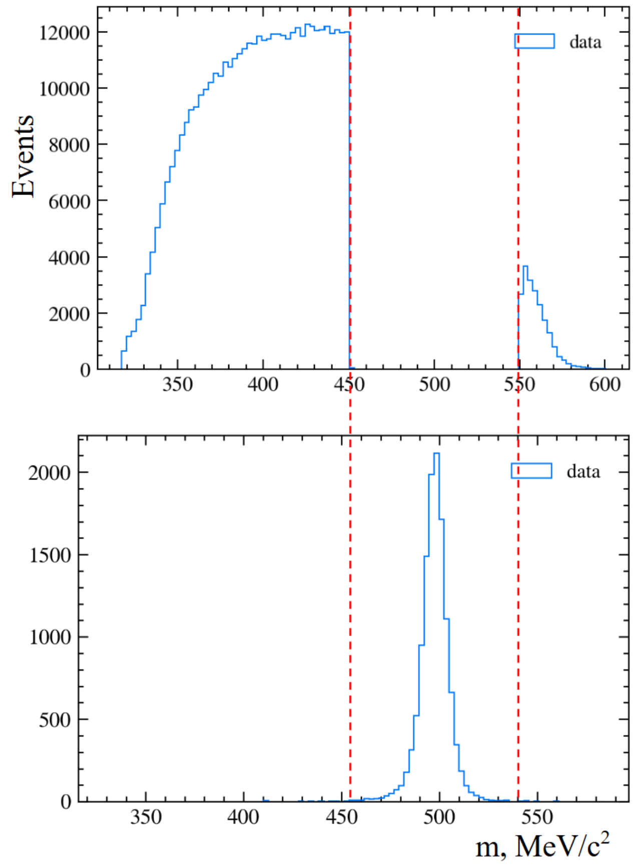

Figure 11: Background suppression effect on the experimental data.

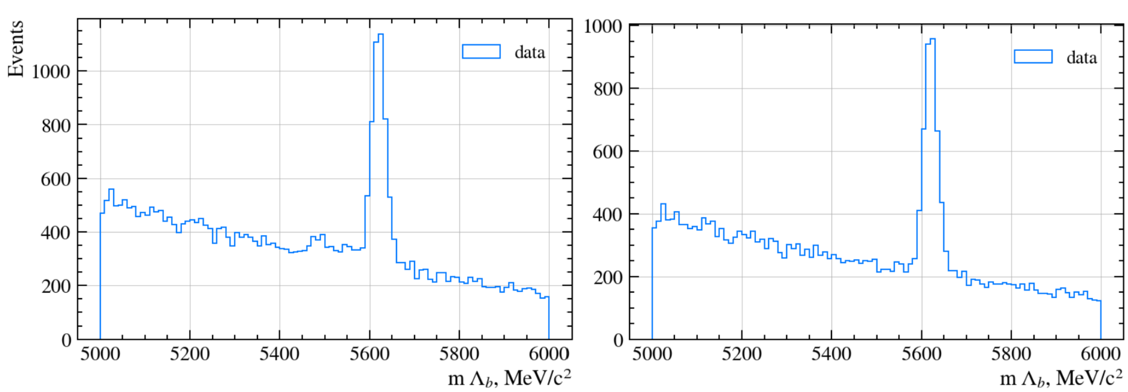

Figure 12: Full dataset Λ_b mass histogram before (left) and after (right) the misID background suppression.

η	(2 , 5)
q^2, MeV^2/c^4	(13.4 , 13.9)
Λ_b mass, MeV/c^2	(5000 , 6000)
K_s^0 invariant mass reconstructed	3σ wide cut

Table 2: The list of selection criteria for Λ_b related events.

Data Set	μ	σ	Reduced χ^2
DDMU	5621.72	16.16	1.15
DDMD	5621.80	16.08	1.26
LLMU	5621.84	15.08	1.12
LLMD	5621.80	15.12	1.19

Table 3: The optimal Gaussian fit parameters calculated for the MC simulations and their respective reduced χ^2 value.

such a way the mean and the standard deviation values are obtained for signal modelling (Table 3). The background is modelled as a decaying exponential. The total fit is the sum of the two models (Equation 3.2).

$$f(x) = Ae^{-(x-\mu)^2/2\sigma^2} + Be^{-\lambda x} \tag{3.2}$$

To fit the events, the data is expressed as a probability density function. After this scaling, the model is produced, where the values for Gaussian normalization factor, exponent normalization factor and the decay constant are fitted. The result of the modelling procedure with the visualisation of individual model contributions is seen in the Figure 14. The Gaussian model is then scaled back to represent the real event numbers.

After the modelling procedure is worked out, it is possible to implement yet another selection criterion to separate the Λ_b and $\bar{\Lambda}_b$ events. This selection is focused on the products of Λ^0 decay, namely a proton-pion pair. A proton and a negatively charged pion are produced in such a decay while $\bar{\Lambda}^0$ produces a positron and a positively charged pion. Using the LHCb particle identification scheme [16] and the DTF proton and pion identification values, the data is separated into Λ_b and $\bar{\Lambda}_b$ events, that are modelled individually. The respective Gaussian normalization factors are translated into the event counts.

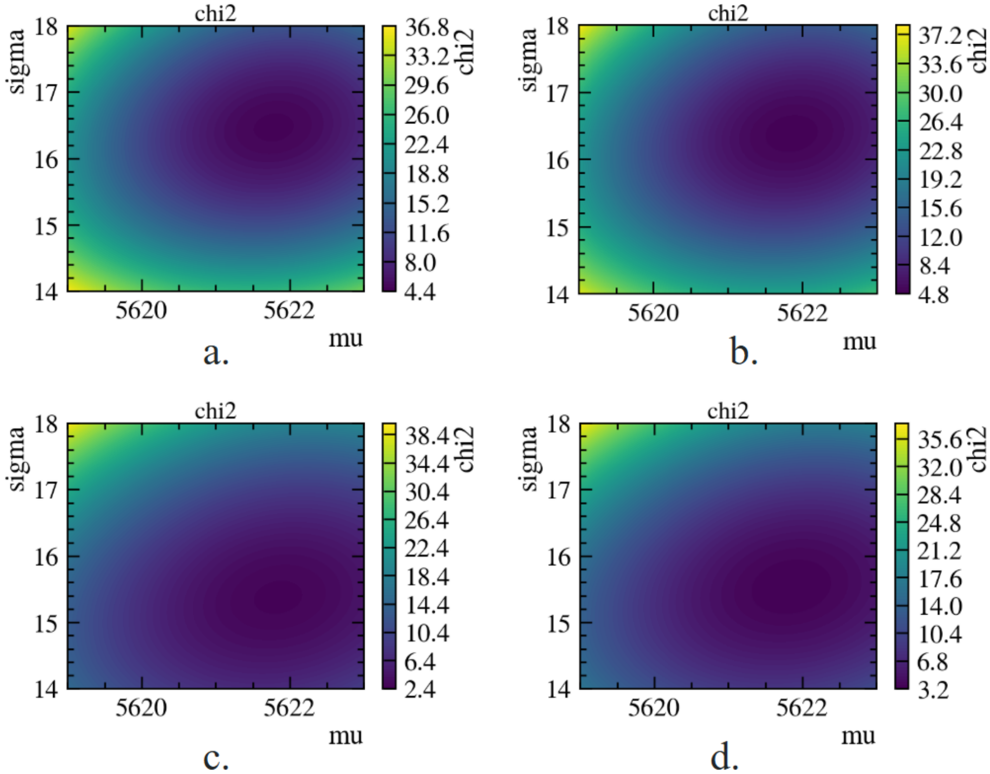

Figure 13: Two-dimensional distributions of reduced χ^2 values for Gaussian fit parameters tested on a) DDMU, b) DDMD, c) LLMU, d) LLMD MC simulation datasets.

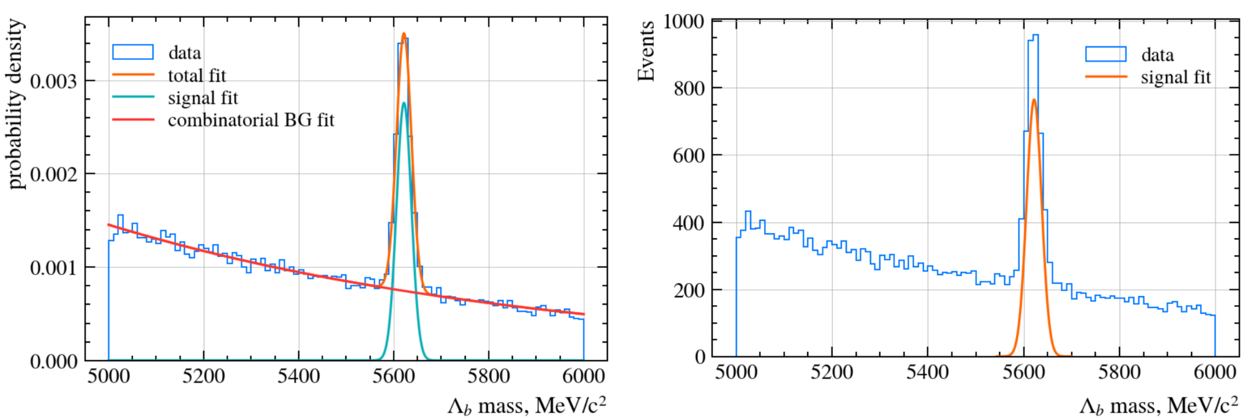

Figure 14: Total PDF model with individual contributions (left) and Gaussian curve scaled to fit the signal events (right).

Data Set	Λ_b events	$\bar{\Lambda}_b$ events	Raw Asymmetry	Z-score
DDMU	445.3 ± 21.2	438.3 ± 21.0	0.008 ± 0.024	0.33
DDMD	459.5 ± 21.5	440.4 ± 21.0	0.021 ± 0.024	0.89
LLMU	324.7 ± 18.1	271.1 ± 16.5	0.090 ± 0.031	2.98
LLMD	293.1 ± 17.2	291.6 ± 17.1	0.003 ± 0.030	0.09
DD	905.3 ± 30.1	879.0 ± 29.5	0.015 ± 0.017	0.88
LL	619.3 ± 24.9	565.6 ± 23.8	0.045 ± 0.021	2.16
Total	1541.3 ± 39.3	1455.3 ± 38.2	0.029 ± 0.014	2.19

Table 4: Result table.

4 Results

Using Monte Carlo simulations of Λ_b decay and 12 datasets for three years of Run 2 (2016-2018) for the MU and MD configurations along the DD and LL tracks, the raw asymmetry of the Λ_b and $\bar{\Lambda}_b$ decay to Λ^0 ($\bar{\Lambda}^0$) and $\psi(2S)$ with subsequent decays to $p\pi^-$ ($\bar{p}\pi^+$) and $\mu\bar{\mu}$ pairs, respectively, is calculated. Models of the Λ_b mass histograms are constructed using a Gaussian signal model and a decaying exponential combinatorial background model. The cut is preliminarily performed to filter out misID signals associated with the K_s^0 decay. The fitting is performed using the Gaussian parameters obtained through the analysis of Monte Carlo simulations and the histograms are scaled to PDF form. The numbers of decay events are obtained based on the Gaussian normalization factor scaled back to the real number of events. The error for the number of counts can be taken from the normalization factor error from the covariance matrix produced for the fit, however, the square root of the counts demonstrates a bigger uncertainty, suggesting that the error value produced by the modelling procedure underestimates the real uncertainty.

The analysis is performed for seven data configurations: four sets for two track types (DD, LL) and two magnet polarities (MU, MD), two data sets that differed in track selection and are concatenated by magnetic field configuration, and the combination of all sets providing the total raw asymmetry (Table 4). The asymmetry value is calculated using the formula (Equation 4.1) (Figure 15), the Z-score is then determined using the ratio (Equation 4.2, Figure 16).

$$A_{raw} = \frac{N_{\Lambda_b} - N_{\bar{\Lambda}_b}}{N_{\Lambda_b} + N_{\bar{\Lambda}_b}} \tag{4.1}$$

$$z = \frac{A_{raw}}{\Delta A_{raw}} \tag{4.2}$$

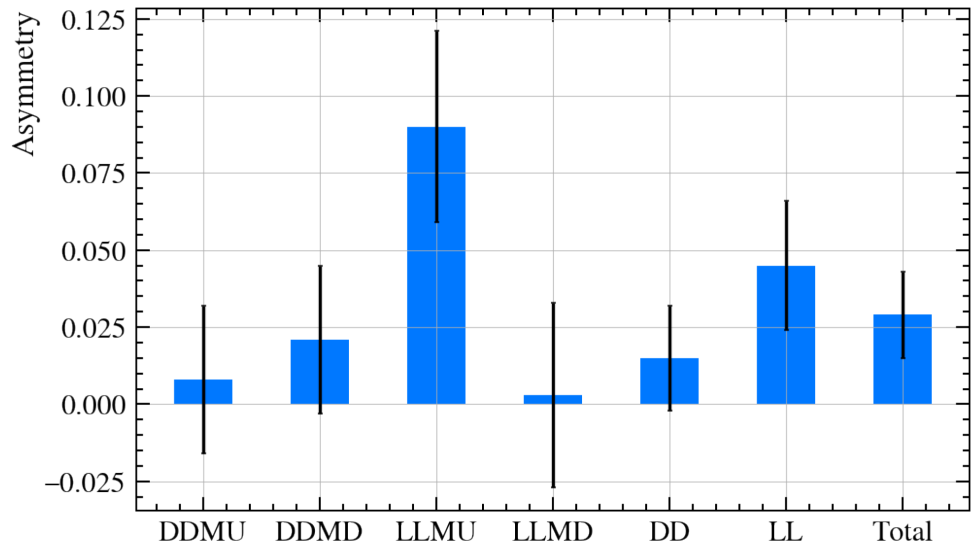

Figure 15: Asymmetry bar graph with uncertainties for all sets and considered dataset combinations.

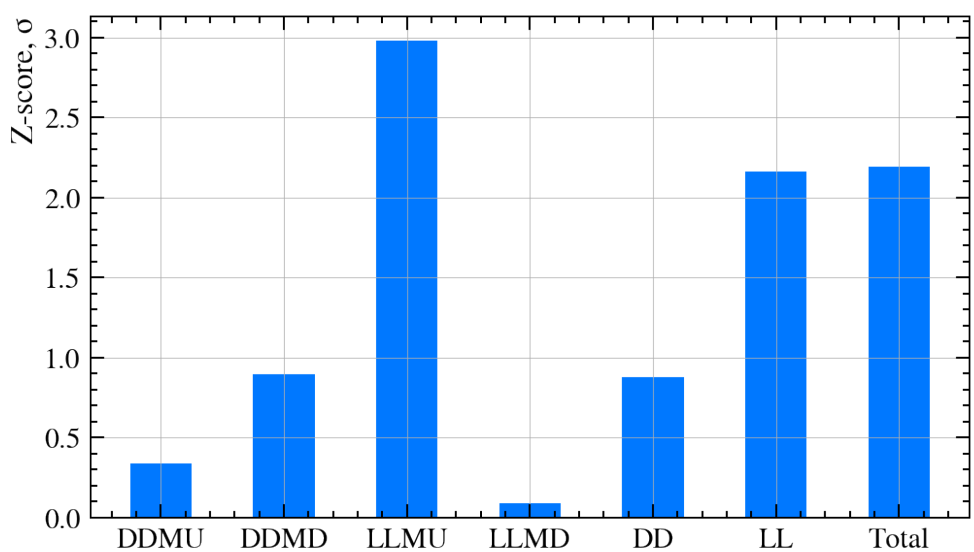

Figure 16: Z-score bar graphs of all sets and considered dataset combinations.

5 Discussion

The modelling procedure with the signal fit parameters predetermined by MC simulations produces a fit that truly reflects the shape of the data presented in the histograms. Being a relatively simple model with an exponential (after misID cut) background and a Gaussian signal, the fit does not correct for the possible asymmetric nature of the background on either side of the signal peak. But given the peak width, even if such an asymmetry is present, its effect is expected to be negligible. Another danger for the calculations may be cut on the misID events, which cannot be completely cut out without a significant loss of signal events. With a 3σ cutoff around the invariant K0s mass, up to 5% of misID events remain, while almost a quarter of signal events are cut off. This ratio of signal-to-background efficiencies is not a good indicator and shows the vulnerability of the analysis to instances of misidentification of particles. The improvement of particle identification techniques can greatly contribute to the study of Λ_b decay. A potential solution for analyzing existing data may be to approximate the region without veto cut, but with the addition of another Gaussian to the model. This will allow more efficient use of the data and simultaneously quantify the scale of the contribution of misID events without sacrificing signal events. The downside of this approach is the divergence from Gaussian distribution in the tails as well as the more complicated modelling process with more fitting parameters, which may offset the positive effect of more extensive statistics.

The obtained raw asymmetry values do not give reason to suspect a significant asymmetry of Λ_b production in the primary vertex or CPV during the decay process. The significance of the asymmetry, taking into account the error, is estimated using the z-score, which in this case is the amount of σ in the deviation from the expected, i.e. from the absence of asymmetry. For the sets concatenated across the magnet states, this value is less than 1 for the DD tracks, but for the LL tracks it shows a 2.16 σ bias, where an asymmetry of 4.5% is recorded. To better understand the reasons, it is necessary to look at the calculations for each individual magnet polarity and track type. Only the LL tracks in the MU configuration show a significant asymmetry of 9% with a 2.98 σ significance. The inconsistency of this result for the other data sets with a high degree of probability points to a source of asymmetry unrelated to the physics of production or decay. The DDMU data collected at the same time show less than one percent asymmetry, further strengthening the assumption that the source lies in the systematic uncertainties, statistical fluctuations, deterioration or other peculiarities of the detector.

Taking into account the above, it is safe to say that CPV is not observed, and the error is significant enough in comparison with the result to call it into question. Even the LLMU set, for all its exceptionality, lies well within 5 σ, while the very fact of its exceptionality makes one doubt the reliability of the result. Further research may focus on finding specific periods when outstanding values of asymmetry in LLMU were obtained.

6 Conclusion

In this study, the raw asymmetry in $\Lambda_b \to \Lambda^0\psi(2S)$ decays was measured using LHCb Run 2 data. No significant CP violation was observed, and the results are in agreement with the Standard Model predictions. The main limitations of the work are related to the absence of a control channel analysis, allowing detector effects to interfere with the measured asymmetry, remaining misID background overlaping with the signal, and statistical uncertainties. Future work may focus on improving selection techniques and increasing the dataset to enhance sensitivity to possible CPV effects in Λ_b decays.

Within the framework of this work, the raw asymmetries were assessed in the decays $\Lambda_b \to \Lambda^0\psi(2S)$ using the LHCb experiment for the Run 2 period. The obtained asymmetry values do not indicate a significant CPV and are in accordance with the predictions of the SM, which allows to use the said channel for normalisation. The applied methods of selecting events and distribution modelling showed their effectiveness, however, the analysis revealed a number of restrictions related to the residual contribution of the misidentification of particles and statistical fluctuations. The main difficulties are associated with the impossibility of complete suppression of background events, as well as the lack of analysis of control channels, which limits the accuracy of accounting for detector effects.

In the future, the development of analysis is possible through the use of the Run 3 data, the PID algorithm enhancement and the expansion of the set of control channels. This will increase the sensitivity to possible instances of CPV. The results and developed methods can be applied in future studies of rare decays of baryons and the search for effects Beyond the Standard Model.

7 Acknowledgements

I would like to express gratitude to my supervisor, Ann-Kathrin Perrevoort, for the support throughout this project. For all the rare instances of me asking for help or a consultation otherwise, she had been there to help.
I am also grateful to the researchers team at KVI for their help with software, finding useful variables for my analysis, coffee brakes, and the positive working atmosphere.
Finally, I thank my family and coursemates for their support during the completion of this thesis.

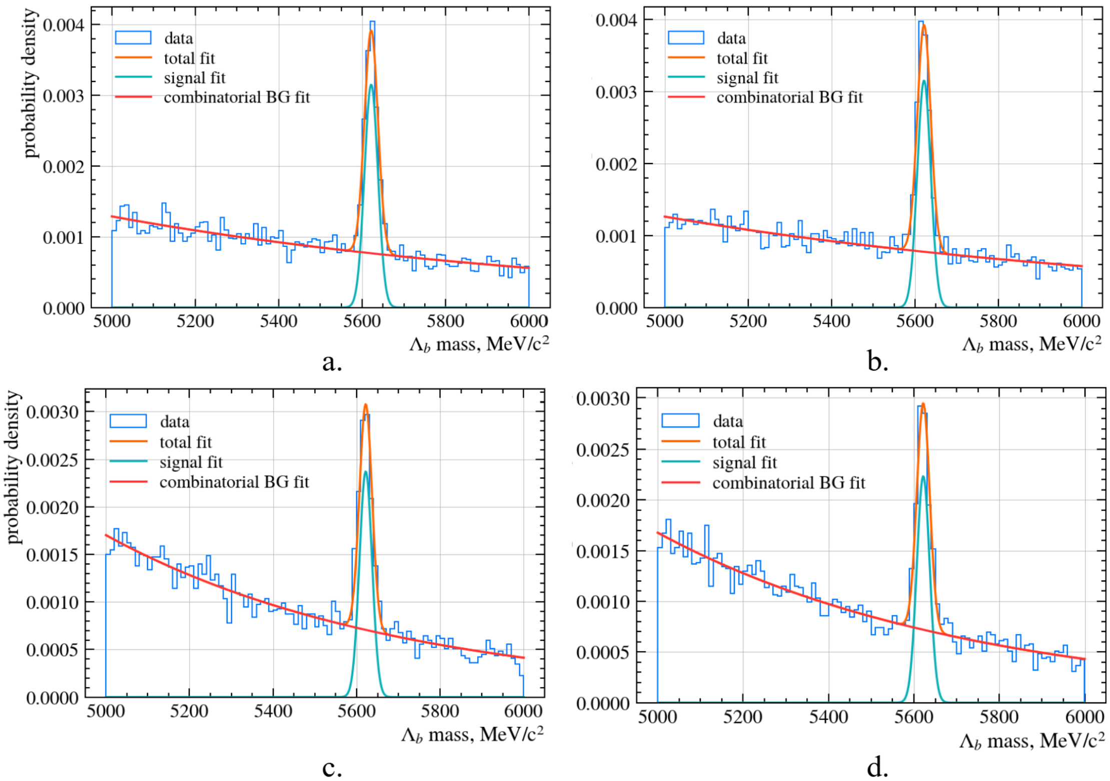

Figure 17: Modelling procedure carried out on a) DDMU, b) DDMD, c) LLMU, d) LLMD datasets.

8 Appendix

8.1 Error Propagation

To calculate the raw uncertainty of the raw asymmetry, the partial derivative method is used (Equation 8.1):

$$\Delta A = \sqrt{\left(\frac{2N_{\bar{\Lambda}_b} \cdot \Delta N_{\bar{\Lambda}_b}}{(N_{\Lambda_b} + N_{\bar{\Lambda}_b})^2}\right)^2 + \left(\frac{2N_{\Lambda_b} \cdot \Delta N_{\Lambda_b}}{(N_{\Lambda_b} + N_{\bar{\Lambda}_b})^2}\right)^2} \tag{8.1}$$

8.2 Figures and Tables

The fits for the individual track type / magnet polarity combinations are shown in the Figure 17:

The detailed result overview is presented in the Table 5:

Data Set	Total events	Veto window, MeV	Λ_b events	$\bar{\Lambda}_b$ events	Asymmetry	Z-score
DDMU	884.0 ± 29.8	(480.18, 514.62)	445.3 ± 21.2	438.3 ± 21.0	0.008 ± 0.024	0.33
DDMD	904.8 ± 30.1	(480.19, 514.81)	459.5 ± 21.5	440.4 ± 21.0	0.021 ± 0.024	0.89
LLMU	597.7 ± 24.5	(487.89, 507.81)	324.7 ± 18.1	271.1 ± 16.5	0.090 ± 0.031	2.98
LLMD	582.1 ± 24.2	(486.89, 508.61)	293.1 ± 17.2	291.6 ± 17.1	0.003 ± 0.030	0.09
DD	1786.4 ± 42.3	(480.19, 514.72)	905.3 ± 30.1	879.0 ± 29.5	0.015 ± 0.017	0.88
LL	1184.8 ± 34.5	(487.39, 508.21)	619.3 ± 24.9	565.6 ± 23.8	0.045 ± 0.021	2.16
Total	2996.6 ± 54.8	(483.79, 511.46)	1541.3 ± 39.3	1455.3 ± 38.2	0.029 ± 0.014	2.19

Table 5: Result overview with the total counts and cut (veto) region for all considered dataset combinations

References

[1] A. D. Sakharov, "Violation of CP in variance, C asymmetry, and Baryon Asymmetry of the Universe," *Soviet Physics Uspekhi*, vol. 34, pp. 392–393, 5 1991. DOI: 10.1070/pu1991v034n05abeh002497. [Online]. Available: https://doi.org/10.1070/pu1991v034n05abeh002497.

[2] P. Chang, K. Chen, and W. Hou, "Flavor physics and CP violation.," *Progress in Particle and Nuclear Physics*, vol. 97, pp. 261–311, 2017. DOI: 10.1016/j.ppnp.2017.07.001. [Online]. Available: https://doi.org/10.1016/j.ppnp.2017.07.001.

[3] CERN. "LHCb." (2025), [Online]. Available: https://home.cern/science/experiments/lhcb.

[4] R. Aaij et al. (LHCb Collaboration), "Differential branching fraction and angular analysis of 0 b → + decays.," *Journal of High Energy Physics*, 2015. DOI: 10.1007/jhep06(2015)115. [Online]. Available: https://doi.org/10.1007/jhep06(2015)115.

[5] D. J. Griffiths, *Introduction to Elementary Particles*, 2nd. Wiley-VCH, 2008.

[6] Wikimedia Commons. "Standard Model of Elementary Particles." (2019), [Online]. Available: https://commons.wikimedia.org/wiki/File:Standard-Model-of-Elementary-Particles.svg..

[7] M. Kobayashi and T. Maskawa, "CP-Violation in the Renormalizable Theory of Weak Interaction," *Prog. Theor. Phys.*, vol. 49, pp. 652–657, 1973. DOI: 10.1143/PTP.49.652.

[8] A. A. Alves Jr. et al. (LHCb Collaboration), "The LHCb detector at the LHC.," *Journal of Instrumentation*, vol. 3, pp. 261–311, 2008. DOI: 10.1088/1748-0221/3/08/s08005. [Online]. Available: https://doi.org/10.1088/1748-0221/3/08/s08005.

[9] CERN. "LHC Report: Another run is over and LS2 has just begun." (2025), [Online]. Available: https://home.cern/news/news/accelerators/lhc-report-another-run-over-and-ls2-has-just-begun.

[10] CERN. "LHC Report: The final days of Run 2." (2025), [Online]. Available: https://home.cern/news/news/accelerators/lhc-report-final-days-run-2.

[11] R. Aaij et al. (LHCb Collaboration), "Measurement of the track reconstruction efficiency at LHCb.," *Journal of Instrumentation*, vol. 10, pp. 392–393, 02 2015. DOI: 10.1088/1748-0221/10/02/p02007. [Online]. Available: https://doi.org/10.1088/1748-0221/10/02/p02007.

[12] Particle Data Group, "Review of Particle Physics," *Prog. Theor. Exp. Phys.*, no. 8, p. 083C01, 2024. DOI: 10.1093/ptep/ptac097.

[13] Z. Rui, C.-Q. Zhang, J.-M. Li, and M.-K. Jia, "Investigating the color-suppressed decays $\Lambda_b \to \Lambda\psi$ in the perturbative qcd approach," *arXiv preprint arXiv:2206.04501*, 2022, hep-ph/2206.04501.

[14] R. Aaij et al. (LHCb Collaboration), "Long-lived particle reconstruction downstream of the LHCb magnet.," *The European Physical Journal C*, vol. 85, 2025. DOI: 10.1140/epjc/s10052-024-13686-6. [Online]. Available: https://doi.org/10.1140/epjc/s10052-024-13686-6.

[15] T. Aaltonen, J. Adelman, T. Akimoto, *et al.*, "First measurement of the ratio of branching fractions $B(\Lambda_b^0 \to \Lambda_c^+ \mu^- \bar{\nu}_\mu)/B(\Lambda_b^0 \to \Lambda_c^+ \pi^-)$," *Physics Research Publications*, vol. 79, DOI: 10.1103/physrevd.79.032001. [Online]. Available: https://doi.org/10.1103/physrevd.79.032001.

[16] L. Garren, I. G. Knowles, T. Sjöstrand, and T. Trippe, "Monte Carlo particle numbering scheme.," *The European Physical Journal C*, vol. 60, pp. 205–207, 3 2000. DOI: 10.1007/bf02683426. [Online]. Available: https://doi.org/10.1007/bf02683426.